IL NUOVO CIMENTO Vol. 36 C, N. 4 Luglio-Agosto 2013
DOI 10.1393/ncc/i2013-11541-3

Communications: SIF Congress 2012

Faraday instability in deformable domains

G. Pucci(*)

Matière et Systèmes Complexes, Université Paris Diderot - Paris 7, CNRS - UMR 7057 Bâtiment Condorcet, 75013 Paris, France and
Dipartimento di Fisica, Università della Calabria - 87036 Rende (CS), Italy

ricevuto il 2 Gennaio 2013

Summary. — Hydrodynamical instabilities are usually studied either in bounded regions or free to grow in space. In this article we review the experimental results of an intermediate situation, in which an instability develops in *deformable* domains. The Faraday instability, which consists in the formation of surface waves on a liquid experiencing a vertical forcing, is triggered in floating liquid lenses playing the role of deformable domains. Faraday waves deform the lenses from the initial circular shape and the *mutual adaptation* of instability patterns with the lens boundary is observed. Two archetypes of behaviour have been found. In the first archetype a stable elongated shape is reached, the wave vector being parallel to the direction of elongation. In the second archetype the waves exceed the response of the lens border and no equilibrium shape is reached. The lens stretches and eventually breaks into fragments that have a complex dynamics. The difference between the two archetypes is explained by the competition between the radiation pressure the waves exert on the lens border and its response due to surface tension.

PACS 47.20.Ma – Interfacial instabilities.
PACS 05.45.-a – Nonlinear dynamics and chaos.
PACS 05.65.+b – Self-organized systems.
PACS 47.35.Pq – Capillary waves.

1. – Introduction

A liquid surface becomes unstable to waves when it experiences vertical oscillations of sufficient amplitude. This instability was discovered by Faraday who observed patterns of standing waves oscillating at half the excitation frequency [1]. It results from the parametric forcing of gravity, a quantity entering the expression of the system eigenfrequency. Benjamin and Ursell wrote the linear theory of the instability that predicts the surface eigenmodes, showing that their excitation is ruled by the Mathieu equation [2].

(*) E-mail: giuseppe.pucci@fis.unical.it

The wave pattern is determined by the shape of the liquid container and the relation between observed patterns and resonant modes of the container was widely investigated by Douady [3]. Recently, a Floquet analysis which takes into account the effect of viscosity [4] and a perturbative treatment of the linear stability problem [5] accounted for the instability threshold and its relation to resonant modes.

The Faraday instability is an example of instability that depends on the geometry of the cell which imposes rigid boundary conditions. The most widely investigated bounded instability is the Rayleigh-Bénard convection, in which a fluid placed between two plates having different temperature develops convection rolls. The typical size of the rolls is the spacing between the plates and the resulting periodic structure adapts to the horizontal dimension of the cell [6, 7]. Another example is the Saffman-Taylor or viscous fingering instability [8] confined by a thickness gradient, which presents periodic fingers. The Saffmann-Taylor instability can also occur in an open circular geometry, where it presents fractal structures [9]. A typical example of free instability is given by thermal plumes, that grow above a heat source and expand spontaneously [10, 11]. In open atmosphere buoyancy effects generate turbulent structures that are free to grow in open space, the boundaries of the turbulent region being given by the dynamics of the turbulent structures. Similar behaviours can be found in crack propagation, solidification etc.

Recently, Pucci *et al.* [12] have reported the experimental observations of an intermediate situation, in which the Faraday instability develops in a *deformable* domain. They triggered the Faraday instability in liquid lenses of weak viscosity floating on a bath of an immiscible liquid of larger viscosity. As the threshold of the Faraday instability increases with the fluid viscosity, it is possible to trigger Faraday waves in the lenses while the bath remains at rest. The waves deform the lenses that behave as deformable domains. The observed steady or unsteady patterns result from the *mutual adaptation* of waves and domain border. Two archetypes of behaviour of such a system have been found. In the first archetype a stable elongated shape is observed as a result of the mutual adaptation. Pucci *et al.* have shown that the elongated shape is the solution of a Riccati equation in which the main ingredients are the wave radiation pressure and the border response due to surface tension [13]. In the second archetype the wave radiation pressure exceeds the possible response of the lens boundary so that no steady regime is reached. The lens is stretched and disrupted by the effect of the waves, forming small fragments that propagate and interact on the bath surface.

In this article we review the experimental findings of Faraday instability in floating liquid lenses. Moreover we discuss the difference between the two archetypes in terms of the dimensionless parameter a_0, which is the ratio of the wave radiation pressure and the border response due to surface tension.

2. – Experimental methods

The basic experimental setup is shown on fig. 1. A cell containing the two fluids is placed on a vibration exciter that forces it to oscillate vertically at fixed frequency in the range $30\,\mathrm{Hz} \leq f_0 \leq 250\,\mathrm{Hz}$. An accelerometer is fixed to the cell and measures the effective sinusoidal acceleration to which the cell is submitted $\gamma(t) = \gamma_m \cos 2\pi f_0 t$. The forcing acceleration range is $0 \leq \gamma_m/g \leq 10$.

Photographs and movies are taken using normal and high-speed videocameras.

Using top views the horizontal shape of the lenses can be investigated and Faraday wavelength is measured as the distance between two crests. The light source is placed horizontally near the vibration exciter and light is reflected vertically to the liquid sur-

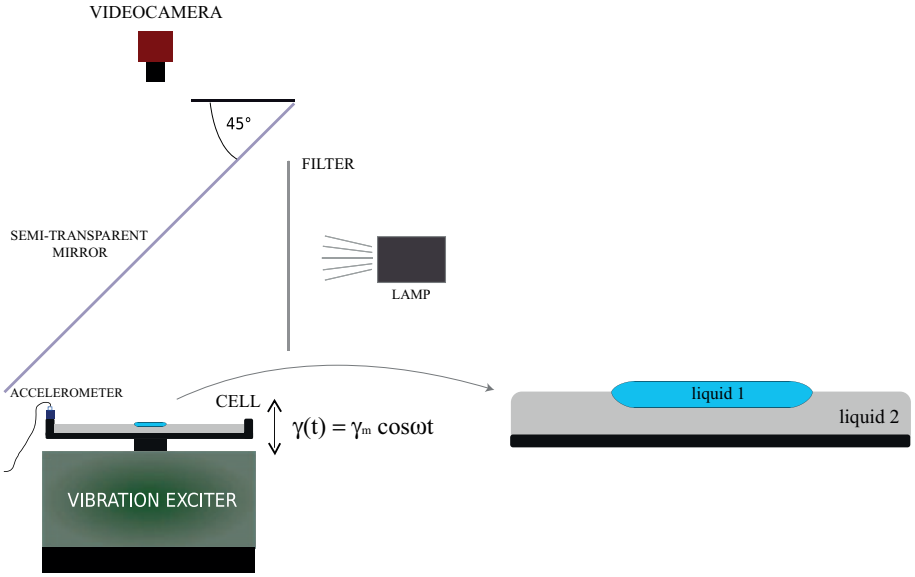

Fig. 1. – Basic experimental setup in the configuration used for top view imaging.

face via a semi-transparent mirror. The videocamera is placed vertically above the cell and records the evolution of the surface topography. In these recordings white regions correspond to horizontal zones of the surface, because they reflect the light beams to the videocamera.

Side views are used to measure wave amplitudes, contact angles and lens thickness. A videocamera is placed in front of the cell and collects the light coming from behind it. In this configuration, transparent plexiglas cells are used in order to observe the emerged and submerged part of the lenses.

The high-speed videocamera (acquisition frequency 2000 Hz) is employed in order to investigate transients.

Much attention is payed to the choice of liquids because they have to satisfy some criteria. In the following we systematically denote by subscript 1 the physical characteristics of floating lenses and by the subscript 2 those of the liquid bath. ρ, σ and μ denote respectively density, surface tension and viscosity.

Liquid 1 and 2 must be immiscible with $\rho_2 > \rho_1$ in order to obtain floating lenses. The shape of floating lenses at rest has been investigated by Langmuir [14] and Noblin [15] and it is given by the equilibrium between hydrostatic and capillary pressure. Moreover a large viscosity contrast $\mu_2 \gg \mu_1$ is required in order to trigger Faraday waves in the lens avoiding significant waves on the bath. As the threshold amplitude of Faraday instability increases with the fluid viscosity, the larger is the contrast of viscosity, the larger will be the range of amplitude for which waves are triggered in the lens only while the bath remains at rest.

The first experiments were performed using water lenses floating on a fluorinated oil bath [16]. By adding surfactant on the lenses, we observed that surface tension played a crucial role in the experiment. As alcohols surface properties are more stable we decided to use them as liquid 1. Moreover, as alcohols evaporate quite rapidly we used closed cells for long-lasting experiments. We tested many pairs of liquids, usually alcohols as liquid 1 and oils as liquid 2, and we found two global archetype of evolution of the system.

In the first archetype waves deform the lens initial circular shape and the system self-adapts to a steady regime. This behaviour is common to many liquid pairs, as for instance ethanol, butanol, pentanol, propanol and water lenses deposited on fluorinated oil baths. We chose to use isopropanol lenses on a viscous fluorinated oil bath because the lens shapes were more stable in a wide range of forcing parameters. Isopropanol has density $\rho_1 = 785\,\mathrm{kg/m}$, surface tension $\sigma_1 = 20.3\,\mathrm{mN/m}$, viscosity $\mu_1 = 2.26\,\mathrm{mPa{\cdot}s}$. The fluorinated oil has density $\rho_2 = 1850\,\mathrm{kg/m}$, surface tension $\sigma_2 = 16.2 \pm 0.3\,\mathrm{mN/m}$, viscosity $\mu_2 = 26\,\mathrm{mPa{\cdot}s}$. The surface tension between the liquids measured by the pendant drop method is $\sigma_{12} = 6.4 \pm 0.1\,\mathrm{mN/m}$.

In the second archetype the wave radiation pressure exceeds the response of the lens border and a complex dynamics is observed. This behaviour is observed for lenses of water and surfactant on fluorinated oil, or the aforementioned alcohols on viscous silicon oils. The most beautiful and various dynamics is observed for ethanol lenses having $\rho_1 = 789\,\mathrm{kg/m}$, surface tension $\sigma_1 = 22.8\,\mathrm{mN/m}$, viscosity $\mu_1 = 0.9\,\mathrm{mPa{\cdot}s}$, floating on silicon oil having $\rho_2 = 965\,\mathrm{kg/m}$, $\sigma_2 = 20.3 \pm 0.3\,\mathrm{mN/m}$, $\mu_2 = 100\,\mathrm{mPa{\cdot}s}$. The surface tension between the liquids measured by the pendant drop method is $\sigma_{12} = 0.7 \pm 0.1\,\mathrm{mN/m}$. Experimentally we observe that the oil covers the lens with a thin film. As a consequence the only surface tension playing a role during the lens deformation is σ_{12}, which corresponds to a very low restoring force.

3. – First archetype

The first archetype is obtained for instance with isopropanol lenses floating on a fluorinated oil bath. In fig. 2 we report phase diagram and snapshots of a lens of volume 1 ml. The phase diagram is in the plane of forcing frequency and amplitude $(f_0, \gamma_m/g)$. The Faraday instability in the deformable domain can be investigated for forcing parameters falling in the area of the phase diagram that is located between the lens and bath Faraday thresholds (respectively, γ_m^D and γ_m^F).

Below the Faraday threshold the lens is circular in the horizontal plane with a flat surface (C). Increasing the forcing amplitude, Faraday waves appear in the lens above a first onset ($\gamma_m \geq \gamma_m^D$). They form complex unsteady patterns that deform the lens, its average shape remaining circular (D). Sometimes we observe that the lens shape is stable and slightly deformed from the initial circle, with definite patterns on it. They are axisymmetric and non-axisymmetric modes, the latter being stabilized by curved Faraday paths. Increasing the amplitude, lens boundary deformations become larger and waves try to elongate the lens in some directions.

Above a second threshold γ_m^E the waves strengthen and organize in one direction. As a result the lens elongates in the direction parallel to the wave vector and this elongation favours a further organization of the waves. By a slow evolution ($t \gg 1/f_0$) the lens reaches a stable elongated shape (E). The wave vector is parallel to the long side of the lens, a behaviour that is similar to Faraday waves in elongated cells [17].

We notice that the area of the phase diagram in which the elongated shape exists increases in width above $f_0 \simeq 110\,\mathrm{Hz}$ (fig. 2). Below this frequency, the shape is perturbed by global modes that are more easily excited because of the low ratio between wavelength and lens size. We focus on the shapes observed for $f_0 \geq 110\,\mathrm{Hz}$. Observations by high-speed videocamera show that waves are standing on the lens surface. As the forcing amplitude increases the lens elongates further.

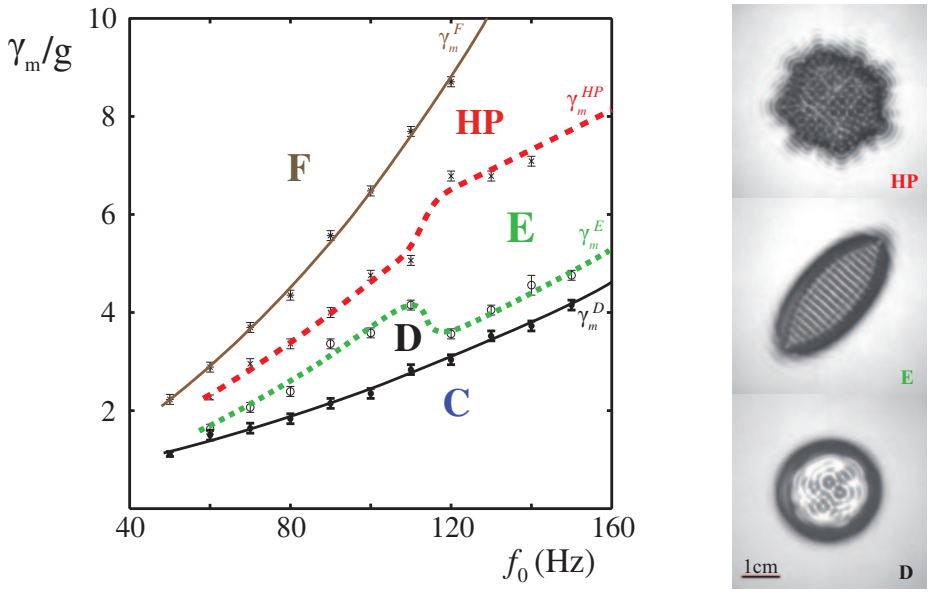

Fig. 2. – Phase diagram and snapshots of an isopropanol lens of volume 1 ml floating on fluorinated oil. C = circular, D = deformed, E = elongated, HP = highly perturbed, F = Faraday instability on the bath. Snapshots of the lens forced at $f_0 = 130\,\mathrm{Hz}$. (D) $\gamma_m/g = 2.94$, (E) $\gamma_m/g = 4.05$, (HP) $\gamma_m/g = 6.43$.

The stable elongated shape is given by the competition between the radiation pressure the waves exert on the lens border and its response due to surface tension. This shape is the solution of a differential equation resulting from the equilibrium between these two effects [13]. The radiation pressure acting on the lens border is a component of the momentum flux density tensor [18] averaged over one period and one wavelength [13]. The approximate border response due to surface tension can be calculated by the Laplace law [18]. We calculate the dimensionless parameter

$$a_0 = \frac{\rho_1 \omega^2 {\zeta_0}^2}{4(\sigma_1/R_0)} \simeq 1, \tag{1}$$

that is the ratio between the two effects, where $\omega = \pi f_0$ is the wave angular frequency. We have taken as typical values of our experiment $f_0 = 100\,\mathrm{Hz}$, the wave amplitude $\zeta_0 \simeq 0.5\,\mathrm{mm}$ and the lens radius at rest $R_0 \simeq 1\,\mathrm{cm}$. $a_0 \simeq 1$ demonstrates that wave radiation pressure and surface tension response are comparable in the first archetype, and this explains the equilibrium.

By increasing the forcing amplitude, ζ_0 and therefore a_0 increase. Experimentally this corresponds to a further elongation of the lens until a new equilibrium is reached. This can be explained by looking at the expression of a_0. As a result of the elongation, the local radius of curvature R_0 at the tips decreases, therefore the restoring force due to surface tension increases too.

Above a third threshold γ_m^{HP} the waves become disordered and the domain experiences large fluctuations (HP). The shape is no longer elongated but circular on time average. Finally at a fourth threshold γ_m^F Faraday waves form on the bath.

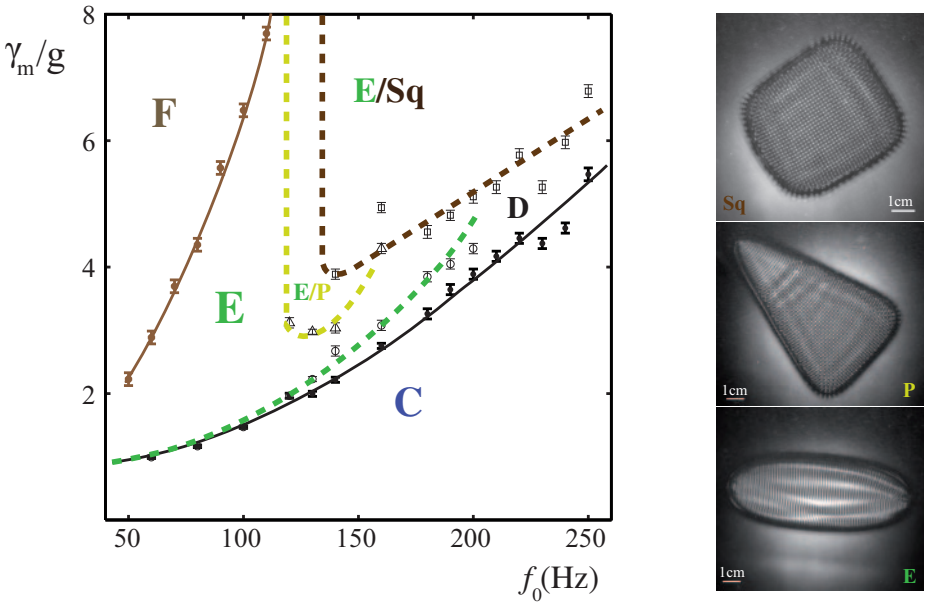

Fig. 3. – Phase diagram and snapshots for a 10 ml floating lens. (C) Circular, (D) deformed, (E) elongated, (P) pear, (Sq) square, (F) Faraday instability in the bath. Snapshots of the lens forced at $f_0 = 160$ Hz. (E) $\gamma_m/g = 3.20$, (P) $\gamma_m/g = 4.29$, (Sq) $\gamma_m/g = 4.90$.

Similar behaviours are observed for much larger lenses (about 10 ml of volume) with the addition of new regimes. We report the results of experiments performed with an isopropanol lens of volume 10 ml. Phase diagram and different regimes are presented in fig. 3.

At low frequencies ($f_0 < 120$ Hz) the lens elongates at the Faraday onset. This occur because the horizontal radius is large and therefore the response of the border is very low. Increasing the amplitude we achieve the Faraday instability in the bath.

At high frequencies ($f_0 \geq 120$ Hz) the lens elongates only above a certain threshold and by increasing rapidly the amplitude two shapes can be observed: a pear shape (P) and a square (Sq). We notice that a slow increase of the amplitude will only lead to a further elongation of the lens (this is why we have E/P and E/Sq areas in the phase diagram) that will exceed the cell size. The elongation process is very slow compared to small lenses and it can last even some minutes until a lens tip reaches the cell walls. Moreover transverse perturbations are observed but they do not affect the global shape. They can be related to scarred patterns observed to compete in the case of a stadium geometry [19].

The pear shape (P) is obtained by increasing rapidly the amplitude. A square pattern takes place but it does not cover the whole lens, so that the waves pushing action continues at least on a tip. The pear usually drifts in the direction of the tip.

If the cell is directly forced by a large amplitude the shape obtained is a square. As the elongated one, this regime is an example of mutual adaptation, but here a square pattern takes place first on the lens while the border remains quite disordered. Successively, the border tries to adapt with a tilted square configuration in which wave vector forms an angle of about 45° with the square sides. This is the shape we expect by adding two

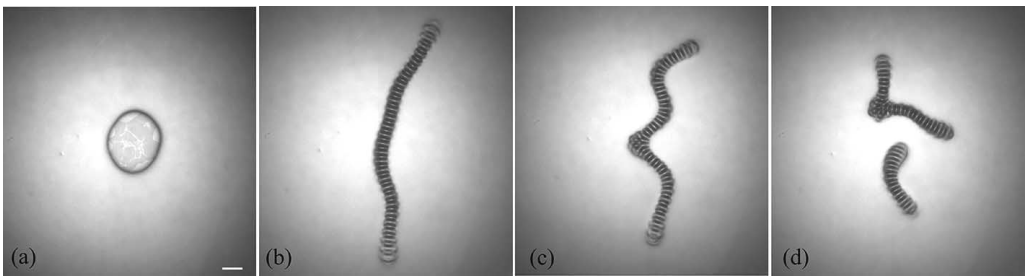

Fig. 4. – Behavior of a 1 ml ethanol lens on silicon oil forced at $f_0 = 100\,\mathrm{Hz}$, $\gamma_m/g = 2.34$ (Faraday threshold). The sequence shows a temporal evolution. Lens at rest before applying the forcing (a). Worms elongation at $t = 17\,\mathrm{s}$ (b), destabilization at $t = 1\,\mathrm{m}\,7\,\mathrm{s}$ (c), breaking at $t = 2\,\mathrm{m}\,22\,\mathrm{s}$ (d). Faraday waves are induced at $t = 0\,\mathrm{s}$ and the bar is 1 cm long.

perpendicular wave fields. However, this configuration is unstable and borders evolves until they are parallel to one wave vector and perpendicular to the other, as shown on fig. 3(Sq). This configuration is only transiently stable because global oscillations of the lens take place destroying the square shape. The system find a new square configuration but global oscillations destabilize it again and so on. We notice that in the mutual adaptation of large lenses the square pattern takes place first, then borders adapt, while in small lenses the mutual adaptation between border and wave pattern is simultaneous. This is because in large lenses the wavelength $\lambda \ll R_0$, so they behave as large cells and present the same pattern observed in a rigid square cavity [3].

4. – Second archetype

In the second archetype a much stronger stretching takes place and it does not lead, at least directly, to an equilibrium situation. Figure 4 shows the evolution at threshold of a lens of ethanol of volume $V \simeq 1\,\mathrm{ml}$ deposited on viscous silicon oil. The surface tension σ_{12} is one order of magnitude lower than that of the first archetype. Moreover the oil covers the lens so that the only surface tension playing a role in the restoring force is σ_{12}. As a consequence we expect that the deformation of the lens boundary due to the action of waves is much stronger. This is exactly what we observe: the formation of parallel standing waves at threshold results into an increasing elongation of the lens into a worm-like structure.

Initially the elongation is approximately straight and wavefronts are perpendicular to the worm's length (fig. 4(b)). At a later stage a kind of buckling occurs and the worm assumes a zigzag shape. During this secondary evolution the wave fronts remain locally perpendicular to the boundaries so that they are no longer parallel to each other. As the amplitude of the zigzag increases, waves in regions of strong curvature become disorganized (c). A new branch starts growing and it pumps liquid out. This process is sometimes so rapid that it empties a part of the old branches and causes the breaking of the worm (d). Two worms are created and they have a dynamic similar to the original worm. The area of the worm increases during the whole stretching process (a, b). As a consequence, the lens thickness decreases during the elongation. The width of the worms is always of the order of the Faraday wavelength.

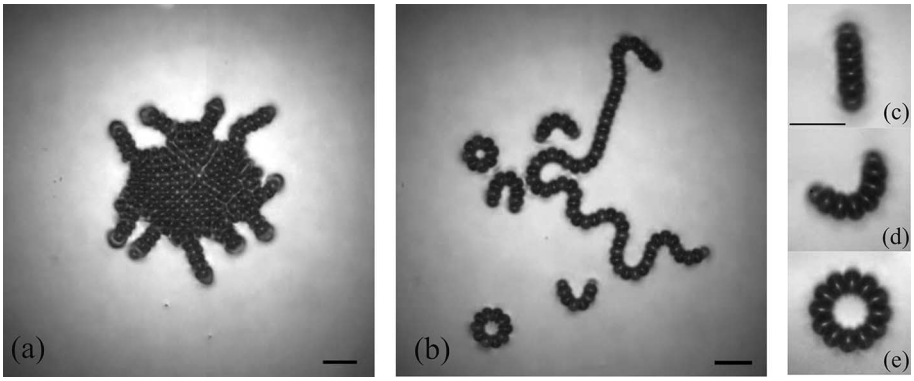

Fig. 5. – Behaviour of a 1 ml ethanol lens on silicon oil forced at $f_0 = 100\,\mathrm{Hz}$, $\gamma_m/g = 6.58$. Snapshot of the lens 1.5 s after the forcing is turned on (a). Aspect of the bath after few minutes of free evolution (b). Typical elongated (c), croissant (d) and ring (e) shape of fragments. Bars are 1 cm long.

This out-of-equilibrium behavior is understood by evaluating again the dimensionless parameter given by the ratio of the wave radiation pressure and the lens border response due to surface tension. Taking the typical values $f_0 = 100\,\mathrm{Hz}$, $\zeta_0 \simeq 0.5\,\mathrm{mm}$, $R_0 \simeq 1\,\mathrm{cm}$ we found

$$a_0 = \frac{\rho_1 \omega^2 {\zeta_0}^2}{4(\sigma_{12}/R_0)} \simeq 100, \tag{2}$$

which shows that the effect of radiation pressure is dominant on the border response.

When a forcing amplitude well above the instability threshold is directly imposed, the dynamics is initially very different (fig. 5). The instability being suddenly triggered in the lens at rest, we first observe the formation of a square pattern of waves. The lens appears to "bud" and "fingers" are observed to grow perpendicular to the sides of the square pattern (a). Some liquid is then transported out of the "body", providing matter for a further elongation of the fingers. The body is thus rapidly destroyed and only an intricate structure of fingers remains. Their dynamics is the same as the branches of the previous case at threshold, but more rapid. The above described dynamics has not lead to an equilibrium situation. Worm-like structures originated by successive breaking keep moving, bending and breaking but they also reconnect when they collide. In practice the bath is covered by moving and motionless fragments that keep colliding, merging and splitting (b). This system is reminiscent of the interplay of structures obtained in cellular automata such as Conway's game of life [20].

The later evolution depends on the confinement imposed by the limited size of the cell. If the initial lens is small and the cell very large the fragmentation will dominate and lead to the formation of small lenses having quasi-equilibrium structures. If the cell is small, lenses during their complex motion come in contact with the menisci bordering the cell and get absorbed by them. In the "dilute case", if we let the system evolve we notice that after a few minutes some small lenses reach equilibrium shapes. They are either simply elongated (c), or in form of croissant (d) and ring (e). Croissant always propagate in the direction of the curvature with constant velocity. They are one more example of self-propagation by a spontaneous symmetry breaking [21].

5. – Conclusion

In this article we have reported the main experimental findings about the Faraday instability triggered in floating liquid lenses. A detailed presentation of the experimental observations can be found in [22]. Liquid lenses behave as deformable domains and a mutual adaptation between the instability pattern and the domain shape is observed. Two different archetypes of behaviour have been found. In the first the mutual adaptation can result in a stable elongated shape with wave vector along the direction of elongation. The stable shape is given by the equilibrium between the radiation pressure of Faraday waves and the restoring effect due to surface tension. For large lenses we have also observed pear and square shapes that are the result of a slightly different adaptation process. In the second archetype the radiation pressure exceeds the restoring effect of surface tension and no stable shape is obtained. The lens is stretched by the waves and can break in several fragments having complex dynamics. These dynamics require further investigations.

The interplay between the waves and the domain border is similar to phenomena of slow self-adaptation of resonant systems, that were observed and studied in particular in two situations. When a wire is loaded by a small sliding mass and set into vibration, the position of the mass adapts so that the whole system is at resonance [23]. A similar situation is observed in vibrating soap films, where the mass distribution adapts to set the film at resonance [24]. The role of the radiation pressure is quite similar to optical cavities, where it creates a coupling between the mirrors degrees of freedom and the optical field [25, 26].

While the aforementioned systems present a self-adaptation due to resonance, in this work the self-adaptation occurs as a consequence of the development of an instability and it is more general. We expect that it shows up in other types of instabilities which are confined by adaptable boundaries.

* * *

This work has been done in collaboration with Yves Couder and Martine Ben Amar and I am grateful to them. I thank Riccardo Barberi for critical reading of the manuscript. Università Italo-Francese (UIF) supported this work.

REFERENCES

[1] Faraday M., *Philos. Trans. R. Soc. London*, **121** (1831) 319.
[2] Benjamin T. B. and Ursell F., *Proc. R. Soc. London A*, **225** (1954) 505.
[3] Douady S., *J. Fluid Mech.*, **221** (1990) 383.
[4] Kumar K. and Tuckerman L. S., *J. Fluid Mech.*, **279** (1994) 49.
[5] Muller H. W., Wittmer H., Wagner C., Albers J. and Knorr K., *Phys. Rev. Lett.*, **78** (1997) 2357.
[6] Bénard H., *Ann. Chem. Phys.*, **7(23)** (1900) 62.
[7] Rayleigh, Lord, *Proc. R. Soc. London A*, **92** (1916) 148.
[8] Saffman P. G. and Taylor G. I., *Proc. R. Soc. London A*, **245** (1958) 312.
[9] Couder Y., *Viscous fingering as an archetype for growth patterns*, in *Perspective in Fluid Dynamics*, edited by Batchelor G. K., Moffat H. K. and Worster M. G. (Cambridge University Press) 2000, pp. 53-104.
[10] Turner J. S., *J. Fluid Mech.*, **13** (1962) 356.
[11] Ben Amar M., *Phys. Fluids A*, **4** (1992) 2641.
[12] Pucci G., Fort E., Ben Amar M. and Couder Y., *Phys. Rev. Lett.*, **106** (2011) 024503.

[13] Pucci G., Ben Amar M. and Couder Y., *J. Fluid Mech.*, **725** (2013) 402.
[14] Langmuir I., *J. Chem. Phys.*, **1** (1933) 756.
[15] Noblin X., Buguin A. and Brochard-Wyart Y., *Langmuir*, **18** (2002) 9350.
[16] Pucci G., *Domain self-adaptation induced by Faraday instability*, Tesi di Laurea, Università della Calabria, 2008.
[17] Douady S., *Instabilité parametrique d'ondes de surface*, PhD Thesis, Université de Paris VI, 1989.
[18] Landau L. D. and Lifshitz E. M., *Fluid Mechanics* (Elsevier) 1987.
[19] Kudrolli A., Abraham M. C. and Gollub J. P., *Phys. Rev. E*, **63** (2001) 026208.
[20] Gardner M., *Sci. Am.*, **223** (1970) 120.
[21] Protière S., Boudaoud A. and Couder Y., *J. Fluid Mech.*, **554** (2006) 85.
[22] Pucci G., *Two phenomena of self-adaptation in out-of-equilibrium systems*, PhD Thesis, Université de Paris VII - Denis Diderot and Università della Calabria, 2011.
[23] Boudaoud A., Couder Y. and Ben Amar M., *Eur. Phys. J. B*, **9** (1999) 159.
[24] Boudaoud A., Couder Y. and Ben Amar M., *Phys. Rev. Lett.*, **82** (1999) 3847.
[25] Meystre P., Wright E. M., McCullen J. D. and Vignes E., *J. Opt. Soc. Am.*, **2** (1985) 1830.
[26] Marquardt F., Harris J. G. E. and Girvin S. M., *Phys. Rev. Lett.*, **96** (2006) 103901.